

Product differentiation during continuous-flow thermal gradient PCR†‡

Niel Crews,^a Carl Wittwer,^b Robert Palais^c and Bruce Gale^{*a}

Received 25th October 2007, Accepted 25th March 2008

First published as an Advance Article on the web 18th April 2008

DOI: 10.1039/b716437h

A continuous-flow PCR microfluidic device was developed in which the target DNA product can be detected and identified during its amplification. This *in situ* characterization potentially eliminates the requirement for further post-PCR analysis. Multiple small targets have been amplified from human genomic DNA, having sizes of 108, 122, and 134 bp. With a DNA dye in the PCR mixture, the amplification and unique melting behavior of each sample is observed from a single fluorescent image. The melting behavior of the amplifying DNA, which depends on its molecular composition, occurs spatially in the thermal gradient PCR device, and can be observed with an optical resolution of 0.1 °C pixel⁻¹. Since many PCR cycles are within the field of view of the CCD camera, melting analysis can be performed at any cycle that contains a significant quantity of amplicon, thereby eliminating the cycle-selection challenges typically associated with continuous-flow PCR microfluidics.

Introduction

The precise melting behavior of double-stranded DNA (ds-DNA) is characteristic of its size, sequence, and molecular composition. A primary factor is the ratio of guanine–cytosine bonds to adenine–thymine bonds, or G–C%. This denaturing of DNA occurs in less than one second over a range of temperatures depending on the G–C content.¹ When the melting of PCR amplicon is monitored with high precision, sequence variations of only a single base pair can be distinguished.^{2,3} Such molecular observations are made by including a ds-DNA dye, LC Green Plus (Idaho Technology, UT, USA), into the PCR mixture, and monitoring its fluorescence over the course of the reaction.⁴ This category of dye emits a greatly intensified fluorescent signal when bound to ds-DNA. As the DNA melts, the dye molecules are released, and the fluorescence dims. During annealing and extension, the dye re-binds to the ds-DNA, and its fluorescence is again enhanced. Thus, with adequate dye concentrations, the fluorescence is proportional to the amount of ds-DNA present at any point within the PCR.

By continuously monitoring the fluorescence during PCR, increasing amplicon concentration can be detected^{5,6} and the temperature *versus* fluorescence relationship during each cycle can be observed. This unique amplicon melting signature can be used to identify the amplified sample.⁴ In many instances,

no further analyses, such as gel or capillary electrophoresis, are needed. This DNA melting analysis technology is used in a growing number of commercial instruments. With several microliters of sample in a stationary capillary tube, these devices uniformly heat the sample while continuously monitoring the change in fluorescence.⁷ This time-dependent DNA melting analysis based on continuous fluorescence acquisition has also been demonstrated with microfluidic systems,^{8,9} although apart from the PCR.

To eliminate the time-dependence of the fluorescence acquisition, the cycles and temperatures of the PCR can be spread spatially instead of over time. A continuous-flow microfluidic PCR device (CF-PCR) has been developed that incorporates constant temperature ramp rates with no cyclic dwell times.¹⁰ This thermocycling protocol is the result of flowing sample through a steady-state thermal gradient established within the substrate. An embedded serpentine channel passes periodically with and then against the direction of heat flow, causing the temperature of the continuously pumped fluid to cyclically rise and fall through the range of PCR temperatures. Since the activity of the DNA polymerase limits the rate of the extension process, the channel width in the heating sections is several times greater than in the cooling sections, resulting in slower fluid velocity and thus a lower rate of sample heating. While the standard CF-PCR configuration allows for the concentration of PCR product to be quantified at each cycle,⁶ this new design has a well-characterized spatial temperature distribution through the transitional temperatures where the DNA amplicon melts. While this earlier thermal gradient PCR study¹⁰ only used end point analysis (gel electrophoresis) to characterize the amplicon after the PCR, the unique temperature profile across the device allows for *in situ* characterization of the amplifying DNA, eliminating the need for most post-PCR processing steps. Mao and coworkers¹¹ have demonstrated the concept of spatial DNA melting analysis from a single image. The thermal gradient PCR device now combines a similar single-acquisition

^aDepartment of Mechanical Engineering, University of Utah, Salt Lake City, UT, 84112, USA. E-mail: gale@mech.utah.edu; Fax: +1 (801) 585-9826; Tel: +1 (801) 585-5944

^bDepartment of Pathology, University of Utah, Salt Lake City, UT, 84112, USA

^cDepartment of Mathematics, University of Utah, Salt Lake City, UT, 84112, USA

† The HTML version of this article has been enhanced with colour images.

‡ Electronic supplementary information (ESI) available: Spatial melting analysis. See DOI: 10.1039/b716437h

fluorescence detection technique and rapid PCR microfluidics, thus making possible the simultaneous amplification, detection, and identification of target DNA fragments.

Experimental

Device fabrication

Using the thermal gradient design, two types of microfluidic chips were fabricated. 30-Cycle PCR chips were manufactured as previously reported.¹⁰ In addition, another type of device was fabricated, whose microfluidic channel incorporates only a single cycle through the temperature gradient. The width and depth of this channel were 600 μm and 100 μm , respectively, with a center-to-center spacing of 3 mm between the counter-flow channel sections. As with the 30-cycle device, this single-cycle channel passed perpendicularly through the gradient over a distance of 10 mm.

A thermal gradient is established in the substrate by placing either device in a heating/cooling apparatus as previously described.¹⁰ To improve upon the uniformity of the spatial temperature distribution, uniform thermal contact was made with the long edges of the PCR chip by using adhesive thermal interface pads (TF-407, Stockwell Elastomerics, Philadelphia, PA, USA). A final power of 6.0 W and 1.18 W was applied to the heaters placed beneath the heated and cooled edges of the chip, respectively, to generate a stable temperature gradient from approximately 60 °C to 95 °C across the 1 cm width of the region through which the microfluidic channel passes. Thermocouples affixed to the glass were used to monitor the range of temperatures, and infrared (IR) thermometry was used to verify and characterize the linearity of the thermal gradient.¹⁰

PCR protocol

The same reagents were used for all PCR samples with the exception of the target-specific primer sequence. A 108-bp section of the human Y-chromosome repeated DNA family DYZ1¹² was amplified, as well as two loci within Cytochrome P-450 2C9,¹³ encompassing exon 3 and exon 7 (CYP2C9*2 and CYP2C9*3, respectively).§ The PCR mixtures contained 5 ng μl^{-1} of male human genomic DNA, 0.5 μM of each primer, 200 mM of each deoxynucleotide triphosphate (dNTP), 0.4 U of KlenTaq1 polymerase (AB Peptides, MO, USA), 6.4 ng of Anti-Taq Monoclonal Antibody (eENZYME LLC, Gaithersburg, MD, USA), 3 mM MgCl_2 , 1X LCGreen Plus (Idaho Technology, UT, USA), and 250 ng ml^{-1} bovine serum albumin (BSA) in a 50 mM Tris (pH 8.3) buffer. The cleaning mixture used between amplification tests contained 15% bleach (Clorox, Oakland, CA, USA) and 2% detergent (7X-O-Matic, ICN Biomedicals, OH, USA). The specific cleaning protocol has been given previously.¹⁰

For the experiments involving the simultaneous amplification and identification of multiple samples, a 90 μl volume of each

sample was prepared, from which 10 μl were removed for amplification on a control system (LightCycler®, Roche, IN, USA). As suggested by Nakayama and co-workers,⁶ a small plug of mineral oil (~20 μl) was first introduced into the chip to reduce bubble formation in the sample, after which the PCR mixture was pumped through the channel at a rate of 1.5 $\mu\text{l min}^{-1}$. After 10 min, when the sample began exiting the chip, the elution was removed in 5 μl aliquots. A minimum of five aliquots was obtained for each PCR sample, after which the PCR mixture remaining in the chip, syringe, and tubing was discarded, and the chip was cleaned prior to injection of a subsequent sample. The serial elutions were analyzed with the control samples on a DNA melting analysis instrument (HR-1, Idaho Technology, UT, USA). In addition, select elutions were also injected into a 1.5% agarose gel for electrophoretic size separation.

For comparison, the single-cycle microfluidic device was used to characterize the spatial melting behavior of the samples amplified on the commercial PCR instrument. 20 μl of each of these PCR mixtures was amplified for 30 cycles on the LightCycler. The three sample plugs were then aspirated into a single syringe, separated by air volumes of 50 μl . A fourth volume (20 μl) of mineral oil was included, which would pass first through the device. The samples were then injected serially through the channel at a rate of approximately 10 $\mu\text{l min}^{-1}$. When a sample completely filled the channel, a fluorescent image was acquired. After the data was obtained for the three samples, the chip and its peripherals were cleaned.

Fluorescence acquisition

To excite the dye in the PCR mixture, the thermal gradient microfluidic devices were operated beneath a ring of royal blue LEDs (455 nm, Luxeon LXH2-BR02, Philips, CA, USA). Since the LC Green Plus dye has an optimum excitation wavelength between 440 nm and 470 nm and emits between 470 nm and 520 nm, the six LEDs were band-gap filtered to 450 \pm 25 nm (HQ450/50X, Chroma Technology Corp, VT, USA). The fluorescence from the PCR samples was detected by an Andor iXon EMCCD camera (DV885JCS-VP, Andor Technology, Belfast, Northern Ireland), which was positioned above the thermal gradient micro-devices. The camera was fitted with an optical lens (EF-S 60 mm f/2.8 Macro USM, Canon Inc., Tokyo, Japan) and a 485 nm long-pass filter (HQ485LP, Chroma Technology Corp, VT, USA). An exposure time of 5 s was used for each acquisition. For the PCR device, a third of the cycles were within the camera's field of view. To detect the change in fluorescence of the microchannel, a background image was taken which was automatically subtracted from the later images. The background was acquired when the initial mineral oil plug filled the channel and the LEDs were illuminating the device. For the simultaneous amplification/detection experiments, a fluorescent image was captured after each 5 μl aliquot was removed from the channel outlet. For the spatial analysis of the pre-amplified sample, one image was taken for each of the three sample volumes.

Spatial melting analysis

The pixel intensity from the acquired fluorescence images was correlated to the approximated temperature distribution

§ The primer sequences for the selected targets are as follows: DYZ1, 108-bp (ATTACTACTACATTCCTTCCA and AGTGAAATTGTATGCAGTAGA) CYP2C9*2, 122-bp (GAATTTGGGATGGGGAA-GAG and TCCAGTAAGGTCAGTGATATGG) CYP2C9*3, 134-bp (CATGCAAGACAGGAGCCA and TGGGAATGAGATAGTTCTGAATTA)

across the chip using a combination of MATLAB™ and LabVIEW™ programming. The raw fluorescence data from each image was filtered for noise reduction and normalized, conducive to a cross-platform comparison of DNA melting experiments.

Results and discussion

Thermal gradient PCR and spatial melting

Fluorescence images of the thermal gradient PCR device were collected for all samples. The first image of each set revealed no fluorescence from the cycles within the camera's field of view. The following image, taken after the first 5 μ l was eluted from the chip, showed a little fluorescence at the early cycles, but still no fluorescence at the final cycles. The fluorescent signal continued to gradually extend down the length of the channel, but at a rate slower than that of fluid flow. After the third sample was removed from the chip, fluorescence was observed at all cycles. This final fluorescence distribution could be considered steady-state, since it remained virtually unchanged for the remainder of the images. Typical images of the device at this state, showing the final 10 cycles of a 30-cycle amplification, are shown in Fig. 1. In this figure as well as the subsequent CCD images, the brightness of the image was adjusted to provide the greatest optical contrast along the length of the channel. Without this adjustment, the brightness of each image is a factor of the size of the target and the initial copy number of the amplified sequence. The cooler regions of the channel emit a brighter signal, even where amplicon levels are not detectable. This is attributed to:

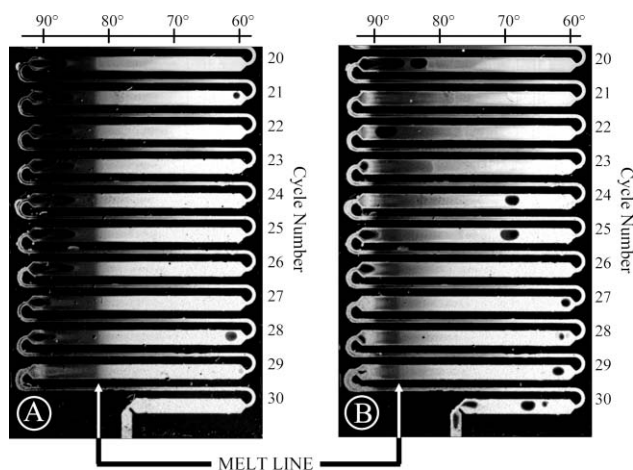


Fig. 1 Fluorescent images of the channel during thermal gradient PCR of the (A) DYZ1, and the (B) CYP2C9*3 targets. The random dark ellipsoids within the channel are slow-moving bubbles. These images show cycles 20 through 30 of a 30-cycle device. As the cycle number increases (top to bottom in the image), the flowing sample continues to amplify. The melting of the amplicon with increasing temperature (right to left in each image) can be seen as a vertical line where the fluorescent signal suddenly fades. The image of the DYZ1 sample shows this “melt line” extending through all visible cycles, indicating that this sample already has a relatively high amplicon concentration after 20 cycles. The melt line for the CYP2C9*3 sample, on the other hand, begins to be visible after 26 amplification cycles, indicating the point at which the CYP2C9*3 amplicon concentration is measurable on this system.

(a) the temperature dependence of the dye fluorescence, and (b) the assumption that full extension of the amplicon occurs very early in the heating stage of each cycle. Within the higher-numbered cycles, a vertical line can be seen where the fluorescence from the heating sample decreases sharply, distinctly indicating the melting of the ds-DNA. By observing the “melt line” from the two images in Fig. 1, it can be seen that the DYZ1 sample has amplified much earlier in the PCR than the CYP2C9*3 sample, since no amplicon melting is observed until cycle 26 for the latter sample. On a PCR device with a high amplification efficiency, the DYZ1 amplicon is expected to reach a measurable concentration approximately 10 cycles faster than the CYP2C9*3 sample, since the target region on the DYZ1 gene is a repetitive sequence, having an estimated 10^3 repeats on each template copy.¹⁴ Images such as that shown in Fig. 1 were obtained for the three DNA targets and a negative control. The final cycles of each PCR are shown in Fig. 2.

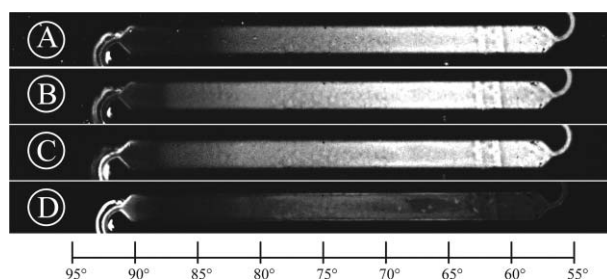


Fig. 2 A comparison of the spatial melting profiles of four amplified samples, which contain: (A) DYZ1 primers with genomic DNA template, (B) CYP2C9*2 primers with genomic template, (C) CYP2C9*3 primers with genomic template, and (D) CYP2C9*2 primers with no template DNA. For the three samples amplified from genomic DNA, the melting of the ds-DNA into ss-DNA can be observed by the extinguishing of the fluorescent signal. The differences in the melting behavior of each sample can be seen. The bright stains seen to the left of each melting zone are likely caused by interactions between the BSA and the fluorescent dye at high temperature.

For comparison, spatial melting curves were also acquired for control samples amplified in the LightCycler. Fig. 3 shows a

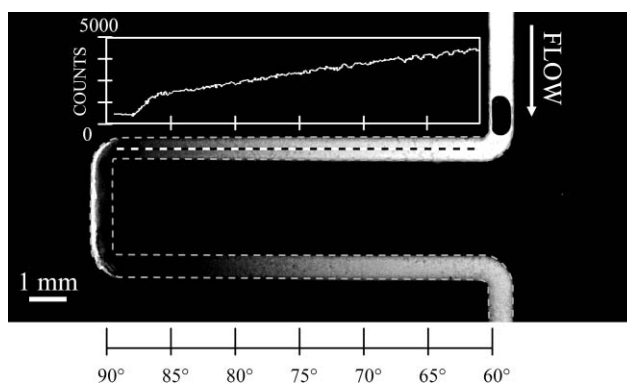


Fig. 3 Fluorescent image of the spatial melting apparatus with an inset graph of the raw fluorescence data along the channel. The CYP2C9*3 sample shown in this image was amplified on the LightCycler. A dashed line outlines the channel, and a dotted line indicates the channel centerline for which the fluorescence plot is shown.

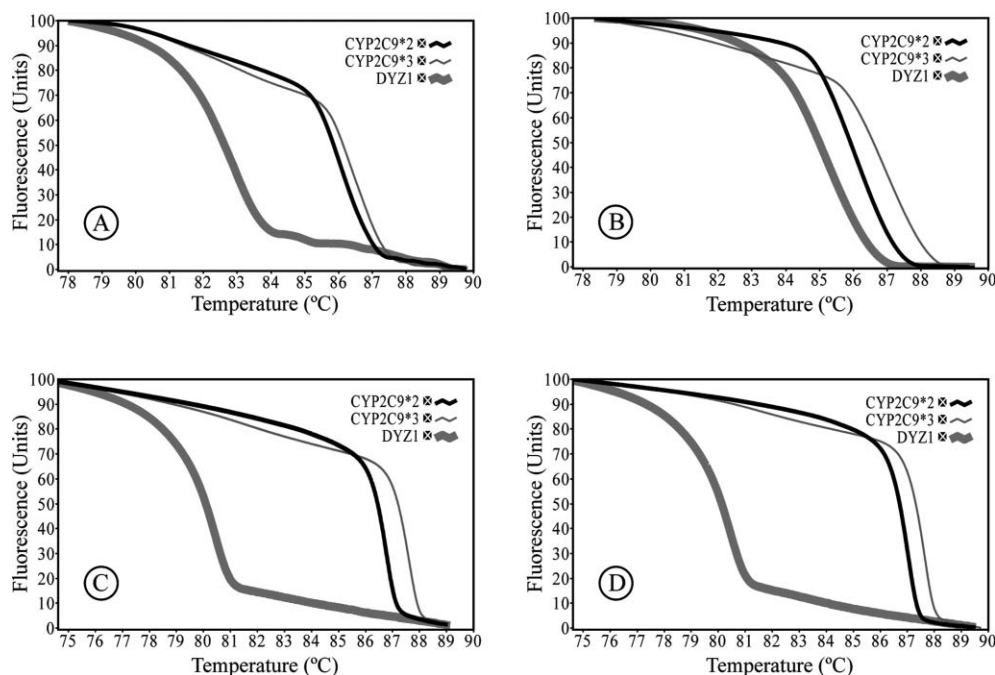


Fig. 4 A comparison of DNA melting curves for the three targets. All curves were processed with the Melting Wizard LabVIEW program. (A) Spatial melting during amplification on the thermal gradient PCR device. These curves plot the images shown in Fig. 2. (B) Samples were amplified on the LightCycler, and then analyzed with the spatial melting device shown in Fig. 3. (C) Samples amplified on the thermal gradient system were melted on the HR-1. These curves were obtained from the 5th elution of each sample. (D) Control samples amplified on the LightCycler and melted on the HR-1.

representative melt of a CYP2C9*3 sample. With this channel design and the temperature distribution as shown, both the denaturing of the amplicon and the subsequent hybridization of the two single strands is observed. Similar images were obtained for all three samples. DNA melting curves were extracted from the spatial melting images shown in Fig. 2, as well as from the image set obtained with the single-cycle melting device. These curves are shown in Fig. 4, along with time-dependent melting curves of samples amplified in the LightCycler and samples amplified in the thermal gradient PCR device. Both data types (from the fluorescent CCD images and from the HR-1) were analyzed. Fig. 4D, which represents the samples that were amplified and melted on the commercial equipment, is the control against which the other graphs should be compared. The curves shown in Fig. 4C, from samples amplified on the microfluidic device and melted on the HR-1, are virtually identical to the control set. The curves obtained from the images taken during microchip PCR, shown in Fig. 4A, show the same melting trends, although the melting temperatures vary from the control by a few degrees. This is attributed to the assumption that a linear temperature gradient exists across the microchannel. While the temperature of the spatial melting curves would become more accurate by incorporating this known non-linearity into the analysis program, the current linear assumption is sufficient to differentiate between the several samples. The curves shown in Fig. 4B are from samples amplified in the LightCycler and melted in the spatial melting microfluidic device. While the three targets can still be distinguished, significant temperature variation is present, as well as some distortion of the melting curve profile. This is attributed to the combination of a faster

flow rate and a greater spacing between the heating and cooling sections of the single-cycle device, which results in a warping of the isothermal lines and a local change in the thermal gradient.

Gel electrophoresis was used to demonstrate the comparable specificity and concentration of the chip-amplified and control samples. Fig. 5 shows this comparison, with amplicon from the two platforms in three sets of adjacent lanes. The vertical agreement between bands and their relative brightness verify that the sizes and concentrations of amplicon generated by the two platforms are nearly identical. It can thus be concluded that the efficiency of the thermal gradient PCR is comparable to that of the LightCycler. Examining the CYP2C9*2 samples

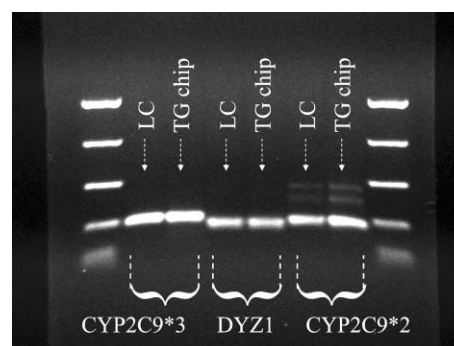


Fig. 5 A gel electropherogram comparing the size, concentration, and specificity of the LightCycler ("LC") and the thermal gradient PCR device ("TG chip") for the amplifications of the CYP2C9*3 (134-mer), the DYZ1 (108-mer), and the CYP2C9*2 (122-mer) targets from human genomic DNA. The samples from the thermal gradient PCR device were all 5th elutions.

shown in this gel, two fainter bands can be seen above the bright primary band. This indicates the unexpected amplification of two additional regions of the DNA. It should be noted that these minor bands were amplified by both systems, which demonstrates the similarities in specificity of the two PCR platforms. Since the size difference of the three amplified targets is slight, the gel electropherogram in the figure required approximately one hour to achieve an observable separation between bands. It can thus be inferred that DNA melting analysis may be preferred over electrophoretic separations for the comparison of multiple samples having similar length.

Channel wall passivation

With 250 ng ml⁻¹ of BSA included in the PCR mixture as a dynamic coating agent, the first several microliters of PCR solution through a cleaned device did not amplify. After approximately 10 µl had passed through the channel, quantifiable amplification began. During the amplification, bright stains also develop in the hottest temperature regions of the channel. Both of these effects are attributed to an initial adsorption of some of the PCR reagents on the walls of the microchannel. It is assumed that this deposition continues until either all binding sites on the glass surface are occupied or until the concentration gradients become large enough to cause the reagent adsorption/desorption rates to equilibrate. This results in significant time and reagent consumption to “prime” the channels before amplification occurs. A number of alternate coating reagents and techniques were also examined. The silanization of the channel walls (Sigma-Cote, Sigma-Aldrich, MO, USA) resulted in the LC Green dye (positively-charged) adhering to the channel walls (negatively-charged). The addition of 0.1–10% Tween 20 (Sigma-Aldrich, MO, USA) to the mixture did not reduce the required priming volume. Neither did the addition of 0.1% (polyethylene glycol) PEG 8000 (Sigma-Aldrich, MO, USA). When PEG was used instead of BSA, amplification did not occur at all. Changes in the concentration of BSA similarly had no effect on the required priming volume. Although incorporating a “priming volume” into the amplification protocol is not preferred, the total time required for amplification and the required sample volumes can be considered satisfactory until the channel modification can be improved. Solutions involving surface modification (chemical treatment to eliminate initial adsorption) and/or priming procedures (reagent flush to induce preparatory adsorption) are being explored.

Device concept

The spatial geometry of the thermal gradient PCR device produces a channel footprint substantially larger than single-well stationary PCR systems,¹⁵ which limits the thermal gradient system's application to perform massively parallel PCR,¹⁶ such as for assays used in drug discovery. This limitation can be overcome by injecting samples in a highly serial manner (*i.e.* sequential small plugs every few seconds). To achieve this, further work must address the current contamination, priming, and data acquisition issues. The current system is capable of rapid, single-sample testing, which, when fully integrated with DNA extraction¹⁷ and sample preparation¹⁸ microfluidics, will be used for the individual genotyping or pathogen detection

of one patient at a time. Small-scale multiplexing of several microfluidic chips could be done to simultaneously analyze a small number of DNA samples or genes, and heating platforms compatible with such operation are currently being considered. These operational characteristics suggest that a fully-integrated device would be best suited for clinical applications such as genotyping related to Warfarin dosing,¹³ pathogen identification related to sepsis detection,¹⁹ and disease diagnosis.²⁰ The thermal gradient chip would be disposable, since the simple manufacturing process would allow mass production at low cost.

There are two features of the thermal gradient PCR device that allow for single-acquisition analysis during product amplification. First, as is characteristic of all CF-PCR devices, the amplification is spread spatially, where each pixel of the channel image corresponds to a certain temperature and cycle number. Secondly, samples passing through this device experience steady temperature ramping, which is unique to the thermal gradient PCR microchip. With a gradient of approximately 3.5 °C mm⁻¹, the field of view used in these experiments provides a resolution better than 0.1 °C pixel⁻¹, which is on the same order of magnitude as the thermal variations within the channel due to convective heat transfer.¹⁰

While these current experiments have used relatively large sample volumes, the PCR components used cost approximately \$0.03 (USD) per microliter.²¹ For high-throughput PCR equipment, reagents generate a significant cost, such that systems requiring smaller reaction volumes provide a strong advantage. However, for the rapid turn-around time, single sample testing to which this current device is suited, moderate volumes are of relatively little expense. Combined with the fact that a single drop of blood contains enough genomic DNA for several hundred microliters of this PCR mixture, reducing the reaction volumes much below 10–20 µl is a negligible improvement.

Each discreet volume of PCR mixture experiences 30 amplification cycles in only 10 min. In a clinical setting, the total time of experiment need not include the insertion of the oil plug or channel priming, since these preparatory steps could be done in advance. Since the sample analysis will be performed *in situ* on a disposable device, a clinical protocol would involve neither the sample removal nor the channel cleaning steps that have been developed as part of this project. In addition, thermal techniques are being explored which will allow for a much faster stabilization of the temperature gradient within the substrate. Doing so would reduce the minimum time between the powering up of such an instrument and its use.

The single-cycle spatial melting device was able to distinguish each of the three samples used in these experiments. Single-acquisition spatial melting of serial sample plugs were obtained with no cleaning of the microchannel. Since the volume of the microchannel where the melting occurs is less than 2 µl, the plug size (20 µl in these experiments) could potentially be reduced by an order of magnitude and still allow for single-acquisition analysis. The required plug size could be further minimized by reducing the channel dimensions. Because of the perturbations observed in the spatial melts on the single-cycle device, the local thermal effects of the flowing fluid on the glass substrate must be characterized and minimized in order to accurately capture the precise melting behavior of the DNA.

Conclusion

Spatial melting analysis of DNA during CF-PCR has been demonstrated. By using thermal gradient PCR to induce steady temperature ramping in the flowing sample, a single image of the fluorescence distribution across the channel can provide sample identification. This ability allows for analysis of the DNA after arbitrary or multiple amplification cycles without disrupting the PCR. Although this technique requires an increase in auxiliary instrumentation, the PCR can now become the final step in the analytical process. This DNA analysis technique has been demonstrated by comparing the amplification of three targets amplified from human genomic DNA. While the melting behavior of each was used to differentiate these samples, further refinement of the system could allow for greater precision in the melting curve acquisition, toward the detection of single nucleotide polymorphisms (SNPs) in the amplifying samples. 30-Cycles of PCR require less than 10 min, which may be further reduced by optimizing the channel geometries and experimental protocols. This simultaneous amplification and detection method, upon incorporating the anticipated improvements in total time and precision/accuracy, will result in a powerful tool for rapid individual DNA testing.

Acknowledgements

Authors credit funding by the State of Utah Center of Excellence program, the University of Utah Synergy Program, and the NSF IGERT Program. Authors thank Rob Stoker for assistance with device testing, Jesse Montgomery for the design of the CYP2C9 primer sets, Scott Sundberg, Rob Pryor, and Oluwole Elenitoba-Johnson for their development of the fluorescence acquisition system, Gundrun Reed for providing the DYZ1 gene primer set, and Luming Zhou and other members of the Wittwer and Gale research labs whose expertise proved of significant value to this project.

References

- 1 C. T. Wittwer, G. B. Reed and K. M. Ririe, in *The Polymerase Chain Reaction*, ed. K. B. Mullis, F. Ferre and R. Gibbs, Springer-Verlag, Deerfield Beach, 1994, pp. 174–181.
- 2 C. T. Wittwer, G. H. Reed, C. N. Gundry, J. G. Vandersteen and R. J. Pryor, *Clin. Chem. (Washington, D. C.)*, 2003, **49**, 853–860.
- 3 L. M. Zhou, L. Wang, R. Palais, R. Pryor and C. T. Wittwer, *Clin. Chem. (Washington, D. C.)*, 2005, **51**, 1770–1777.
- 4 K. M. Ririe, R. P. Rasmussen and C. T. Wittwer, *Anal. Biochem.*, 1997, **245**, 154–160.
- 5 R. Higuchi, *Bio/Technology*, 1993, **11**, 1026.
- 6 T. Nakayama, Y. Kurosawa, S. Furui, K. Kerman, M. Kobayashi, S. R. Rao, Y. Yonezawa, K. Nakano, A. Hino, S. Yamamura, Y. Takamura and E. Tamiya, *Anal. Bioanal. Chem.*, 2006, **386**, 1327–1333.
- 7 M. G. Herrmann, J. D. Durtschi, L. K. Bromley, C. T. Wittwer and K. V. Voelkerding, *Clin. Chem. (Washington, D. C.)*, 2006, **52**, 494–503.
- 8 P. Neuzil, J. Pipper and T. M. Hsieh, *Mol. Biosyst.*, 2006, **2**, 292–298.
- 9 C. Zhang, J. Xu, W. Ma and W. Zheng, *Biotechnol. Adv.*, 2006, **24**, 243–284.
- 10 N. Crews, C. Wittwer and B. Gale, *Biomed. Microdev.*, 2008, **10**, 187–195.
- 11 H. B. Mao, M. A. Holden, M. You and P. S. Cremer, *Anal. Chem.*, 2002, **74**, 5071–5075.
- 12 Y. Nakahori, K. Mitani, M. Yamada and Y. Nakagome, *Nucleic Acids Res.*, 1986, **14**, 7569–7580.
- 13 C. E. Hill, A. Duncan, D. Wirth and F. S. Nolte, *Am. J. Clin. Pathol.*, 2006, **125**, 584–591.
- 14 A. H. Handyside, E. H. Kontogianni, K. Hardy and R. M. L. Winston, *Nature*, 1990, **344**, 768–770.
- 15 M. A. Northrup, B. Bennett, D. Hadley, P. Landre, S. Lehew, J. Richards and P. Stratton, *Anal. Chem.*, 1998, **70**, 918–922.
- 16 T. Morrison, J. Hurley, J. Garcia, K. Yoder, A. Katz, D. Roberts, J. Cho, T. Kanigan, S. E. Ilyin, D. Horowitz, J. M. Dixon and C. J. H. Brenan, *Nucleic Acids Res.*, 2006, **34**, e123–.
- 17 W. Cao, C. J. Easley, J. P. Ferrance and J. P. Landers, *Anal. Chem.*, 2006, **78**, 7222–7228.
- 18 P. Garstecki, M. J. Fuerstman, M. A. Fischbach, S. K. Sia and G. M. Whitesides, *Lab Chip*, 2006, **6**, 207–212.
- 19 G. S. Martin, D. M. Mannino, S. Eaton and M. Moss, *New Engl. J. Med.*, 2003, **348**, 1546–1554.
- 20 C. D. Chin, V. Linder and S. K. Sia, *Lab Chip*, 2007, **7**, 41–57.
- 21 J. Montgomery, J. Kent, C. T. Wittwer and L. Zhou, *Clin. Chem. (Washington, D. C.)*, 2007, **53**, 1891–1898.